JOURNAL OF GEOPHYSICAL RESEARCH, VOL. 103, NO. D20, PAGES 26,127–26,136, OCTOBER 27, 1998

Simulation of enclosure-based methods for measuring gas emissions from soil to the atmosphere

Fang Gao

Air Quality Management Section, Delaware Department of Natural Resources and Environmental Control, Dover

Scott R. Yates

Physics and Pesticide Unit, U.S. Salinity Laboratory, U.S. Department of Agriculture, Riverside, California

Abstract. Enclosure-based methods (i.e., flux chambers) have been widely used in agricultural, ecological, geophysical, and engineering studies to estimate gas exchanges at the soil-atmosphere and the water-atmosphere interfaces. In this study, the flux chambers are analyzed using diffusion theory and mass balance principle. Mathematical models are developed to simulate the general behavior of both closed and dynamic chambers. Simulation for the closed chamber behavior shows that the flux from the enclosed soil matrix into the chamber decreases with time after chamber placement. This indicates that application of a simple linear model to calculate flux may underestimate the real flux, even though the concentration data obtained from the chamber headspace shows a relatively linear increase with respect to time. It is recommended that nonlinear models be considered whenever possible for calculating flux for closed chambers. Simulations of dynamic chambers show that (1) these chambers can reach a steady state rapidly after placement and (2) the proper measurement of flux depends on both chamber operational conditions and soil permeability to air. A dynamic chamber may underestimate the actual flux when operating on low permeable soils. On soils with high air permeability a dynamic chamber may give an underestimate of the actual flux when operating at low airflow rate but an overestimate when the airflow rate is high. Theoretically, both closed and dynamic chambers may produce accurate flux estimates if they operate under ideal conditions and appropriated models are used in flux calculations. In practice, however, a dynamic chamber should be more desirable.

1. Introduction

Enclosure-based methods have been used extensively in scientific research and engineering practice to estimate gas exchanges at the soil-atmosphere and the water-atmosphere interfaces. These methods were first applied and are continuously applied now in agricultural and ecological fields to measure emissions of gases, such as CO_2, N_2O, NO_x, CH_4, and some nonmethane organic compounds, from soil to the atmosphere [*Kanemasu et al.*, 1974; *Denmead*, 1979; *Matthias et al.*, 1980; *Cicerone and Shetter*, 1981; *Holzapfel-Pschorn and Seiler*, 1986; *Moore and Roulet*, 1991; *Rochette et al.*, 1992; *Valente et al.*, 1995; *Fukui and Doskey*, 1996]. In the last decade or so, these methods have found wide application not only in the traditional agricultural, ecological, and geophysical studies but also in environmental investigations and engineering practice to measure emissions of volatile organic compounds (VOCs), such as volatile pesticides [e.g., *Clendening*, 1988; *Yagi et al.*, 1993; *Yates et al.*, 1996], spilled volatile solvents and volatile constituents from waste disposal sites [e.g., *Sanders et al.*, 1985; *Dupont and Reinman*, 1986; *Balfour et al.*, 1987; *Woodrow and Seiber*, 1991], and even gaseous metal or metalloid compounds, such as Se compounds [*Frankenberger and Karlson*, 1994].

Paper number 98JD01345.
0148-0227/98/98JD-01345$09.00

In general, the enclosure-based methods include closed flux chambers (also called static, or passive chambers), and dynamic flux chambers (also called flow-through or active chambers). The closed chambers are usually used in the field to conduct intermittent measurements of the target gas emission. Their placement time is usually short, typically from several minutes to several tens of minutes, as compared to the entire period of emission scenario of interest. The dynamic chambers, on the other hand, are usually operating in the field to monitor the target gas emission continuously over an extended time period. However, the gas samples taken from a dynamic chamber represent the strength of emission from the covered soil in a short period of time, from seconds to hours, depending on the sampling protocol used. The sampling time frame is also very short if compared to the entire emission period of interest, which is usually from days to weeks, or even to months.

Reviews of both closed and dynamic chambers are available [e.g., *Rolston*, 1986; *Wesely et al.*, 1989; *Denmead and Raupach*, 1993]. Experiences gained from numerous applications of both flux chambers have shown that both methods have their own advantages and disadvantages. For closed chambers, one obvious advantage is their simplicity in fabrication and operation. The major disadvantage of using a closed chamber is that the enclosed microenvironment above the soil surface becomes different from that outside the chamber after the chamber placement. Since the interior of the closed chamber is isolated, the concentration of the target gas in the chamber headspace

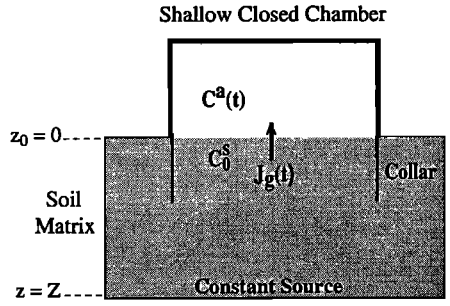

Figure 1. Schematic of shallow closed (passive) flux chamber and soil matrix.

increases with time due to the mass input at the enclosed soil surface. In general, the concentration increase is nonlinear, and some nonlinear models can be used to calculate the flux [e.g., *Hutchinson and Mosier*, 1981; *de Mello and Hines*, 1994]. Oftentimes, the concentration data show a relatively linear relation with respect to time, and a simple linear model has been used to calculate the flux. However, application of the linear model has been reported to lead to underestimate of the actual flux [*Rolston*, 1986; *Wesely et al.*, 1989].

For dynamic chambers, a commonly acknowledged advantage is the possibility of maintaining conditions within the chamber nearly the same as those in the surrounding field. In addition, the problem of a significant concentration buildup of the target gas within the chamber headspace can be avoided, since an airstream (usually clean air) is continuously flowing through these chambers [*Rolston*, 1986; *Yates et al.*, 1996]. When a dynamic chamber operates at a constant airflow rate, a simple steady-state model derived from the mass balance concept can be used to calculate the flux [*Denmead*, 1979; *Rolston*, 1986; *Gao et al.*, 1997]. For the dynamic chambers, introducing an airstream through the chamber may create a pressure deficit within the chamber headspace, which is often cited to induce an additional convective mass flow of the target gas from the covered soil matrix into the chamber headspace. Thus the steady-state flux measured by the dynamic chamber may be an overestimate of the diffusion-driven flux [*Kanemasu et al.*, 1974; *Rolston*, 1986; *Mosier*, 1989].

In this study we analyze both closed and dynamic flux chambers using the diffusion theory and the mass balance principle. For the dynamic chambers, our analysis and simulation are obtained by defining a special chamber structure. Our purpose is to develop relatively simple physical and mathematical models to simulate general behavior of both closed and dynamic chambers and to locate physical (or structural) and operational factors that affect accurate flux measurements. Through these simulations, we can obtain a better understanding of the chambers behavior, the associated problems, and how to improve chamber operation to obtain unbiased or less biased flux measurements.

2. Theoretical Analysis

2.1. Analysis of Shallow Closed Chamber

The common shallow closed chambers have a vertical dimension (i.e., thickness or height) smaller or not significantly greater than their horizontal dimensions (i.e., width and length, or diameter for circular chambers). A schematic diagram of a shallow closed chamber placed at soil surface is shown in Figure 1. The chamber volume is V (L^3), and the covered soil surface area is A (L^2). To simplify our analysis, we make the following assumptions:

1. Chamber placement time is relatively short, usually from several minutes to several tens of minutes. In comparison, the entire emission period of interest is significantly longer, usually from days to weeks, or even months.
2. Before placement the concentration of the target gas in the chamber is zero. In practice, an exact initial zero concentration may be difficult to obtain, and using an ambient initial concentration may be more practical. During the short placement time, there is no sink or degradation process for the target gas within the chamber.
3. During the chamber placement time, the strength of the gas source at a depth of Z (L) below the soil surface is relatively constant. Similar assumptions of a constant source have been used previously by a few investigators in their theoretical studies [*Jury et al.*, 1982; *Healy et al.*, 1996].
4. The flux of the target gas at the enclosed soil surface, $J_g(t)$ ($M L^{-2} T^{-1}$), is uniform at the enclosed soil surface and caused by diffusion which is driven by the concentration gradient across the soil-air interface. This diffusion-driven flux can be given as

$$J_g(t) = h[C_0^s(t) - C^a(t)] \tag{1}$$

where $C_0^s(t)$ ($M L^{-3}$) is the target gas concentration at the soil-atmosphere interface on the soil side, $C^a(t)$ ($M L^{-3}$) is the spatially averaged concentration of target gas in the chamber headspace, and h ($L T^{-1}$) is the transport coefficient of the target gas through the soil-air interface. This coefficient represents the degree of ease in which the target gas can diffuse through the interface, which depends on both the resistant nature of the interface and the diffusivity of the target gas.

The mass change of the target gas within the chamber headspace is due to the emission of the target gas from the covered soil matrix into the chamber headspace

$$dM(t) = V\,dC^a(t) = AJ_g(t)\,dt \tag{2}$$

where A (L^2) is the enclosed soil surface area. Introducing (1) into (2) gives a first-order nonhomogeneous differential equation for $C^a(t)$

$$\frac{dC^a(t)}{dt} + \frac{h}{V/A}\,C^a(t) = \frac{h}{V/A}\,C_0^s(t) \tag{3}$$

where the ratio of V/A will be the chamber height H (L), if the chamber has a uniform cross-section area equal to the enclosed soil surface area. Equation (3) has an initial condition of

$$C^a(0) = 0,\ t = 0 \tag{4}$$

With this condition, (1) becomes

$$J_g(0) = J_0 = hC_0^s(0) \tag{5}$$

which is the flux at the very beginning of the chamber placement. We define this flux to be the initial flux to be measured by the chamber under the given conditions.

The solution of (3) depends on the form of the nonhomogeneous term $C_0^s(t)$. For simplicity and simulation purpose we further assume that $C_0^s(t) = C_0^s$ is a constant during the relatively short chamber placement period. In practice, this situation exists when there is an apparent transport barrier at the soil-atmosphere interface, such as a tarp over a fumigated

agricultural field [*Yates et al.*, 1996]. For this situation the term h is mainly determined by the transport of the target gas through the interfacial barrier. Within the time frame of chamber placement, a tarped fumigated field can be treated as an example of this special situation. With the assumption of a constant $C_0^s(t) = C_0^s$, we can solve (3) and (4) for $C^a(t)$ and obtain

$$C^a(t) = C_0^s \left[1 - \exp\left(-\frac{h}{V/A}\, t \right) \right] \tag{6}$$

which can be then used in (1) to solve for $J_g(t)$

$$J_g(t) = J_0 \exp\left(-\frac{h}{V/A}\, t \right) \tag{7}$$

where J_0 is the flux at $t = 0$, as defined in (5). From (6) and (7) it can be seen that $C^a(t)$ increases with time, and $J_g(t)$ decreases with time. When the chamber placement time is extended, or mathematically when $t \to \infty$, we can have

$$C^a(t) = C_0^s, \qquad t \to \infty \tag{8}$$

$$J_g(t) = 0, \qquad t \to \infty \tag{9}$$

2.2. Analysis of Dynamic Chamber

A schematic diagram of a dynamic (or flow through) chamber placed at soil surface is shown in Figure 2, where we define a square or rectangular chamber to simplify our analysis. The height of the chamber is H (L), the width is W (L), and the length is L (L). The enclosed soil surface area is A (L^2). An important feature of this chamber structure is that the airstream sweeps over the entire covered soil surface with a uniform velocity (V_0, $L\ T^{-1}$) at a given flow rate (Q, $L^3\ T^{-1}$), from the inlet side to the opposite outlet side (Figure 2a) [*Gao et al.*, 1997].

For our dynamic chamber we apply the same assumptions as for the closed chamber. In addition, we assume that the direction of airstream is parallel to the enclosed soil surface (Figure 2), so the velocity of the airstream V_0 ($L\ T^{-1}$) can be estimated using the airflow rate (Q, $L^3\ T^{-1}$) and the chamber dimensions (H and W)

$$V_0 = \frac{Q}{WH} \tag{10}$$

An often cited problem of dynamic chambers is that the flowing air through the chamber may create a pressure deficit in the chamber, which will cause an advective mass transport of the target gas out from the covered soil matrix into the chamber headspace [*Kanemasu et al.*, 1974; *Rolston*, 1986; *Mosier*, 1989; *Wesely et al.*, 1989]. We first analyze a simple case without considering the effect of pressure deficit. Later, we will discuss a more general situation where the effect of pressure deficit is included.

2.2.1. Without effect of pressure deficit. The mass change of the target gas within the chamber headspace is due to the mass input and output, which can be expressed as

$$dM = V\, dC^a(t) = AJ_g(t)\, dt + QC_{in}(t)\, dt - QC_{out}(t)\, dt \tag{11}$$

where $C_{in}(t)$ and $C_{out}(t)$ ($M\ L^{-3}$) are the target gas concentrations in the chamber incoming air and outgoing air, respectively, and other terms are defined previously. Assuming $C_{out}(t) = C^a(t)$ and $C_{in}(t) = 0$ for simplicity, we can obtain

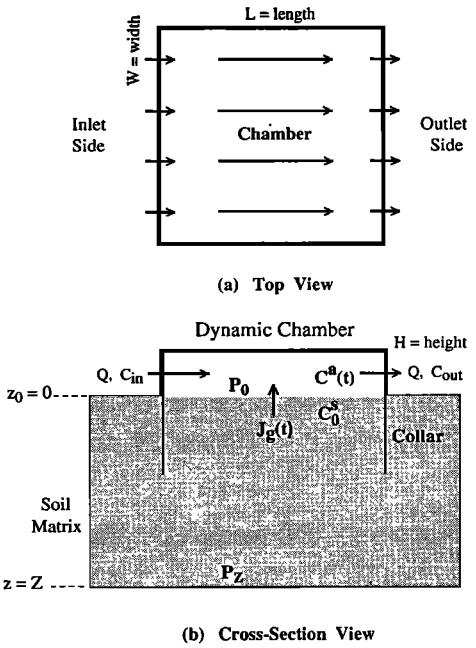

Figure 2. Schematic of dynamic (flow through) flux chamber and soil matrix.

$$J_g(t) = \frac{V}{A}\frac{dC^a(t)}{dt} + \frac{Q}{A}C^a(t) \tag{12}$$

Combining (1) and (12) and noting $V/A = H$ for our dynamic chamber, a first-order nonhomogeneous differential equation for $C^a(t)$ can be obtained

$$\frac{dC^a(t)}{dt} + \frac{Q/A + h}{H}C^a(t) = \frac{h}{H}C_0^s(t) \tag{13}$$

which has an initial condition of

$$C^a(0) = 0, \quad t = 0 \tag{14}$$

The solution of (13) and (14) with the assumption of $C_0^s(t) = C_0^s$ = constant is

$$C^a(t) = \frac{hC_0^s}{Q/A + h}\left[1 - \exp\left(-\frac{Q/A + h}{H}\, t \right) \right] \tag{15}$$

Further, substituting (15) into (1) leads to an expression for the flux at the enclosed soil surface

$$J_g(t) = J_0\left\{ 1 - \frac{h}{Q/A + h}\left[1 - \exp\left(-\frac{Q/A + h}{H}\, t \right) \right] \right\} \tag{16}$$

When the dynamic chamber system reaches a steady state (i.e., $t \to \infty$), (16) becomes

$$J_g(t \to \infty) = J_{steady} = J_0\left(1 - \frac{h}{Q/A + h} \right) \tag{17}$$

Since the term $(1 - h/(Q/A + h))$ is less than 1, (17) indicates that the steady state flux (J_{steady}) is smaller than the initial flux (J_0) at $t = 0$ under the given conditions.

At steady state, or when $t \to \infty$, the target gas concentration within the chamber headspace becomes a constant, which is

$$C^a(t \to \infty) = C_{steady} = C_0^s \frac{h}{Q/A + h} \tag{18}$$

Since $h/(Q/A + h) < 1$, the steady-state concentration (C_{steady}) is less than C_0^s.

Combining (17) and (18) and noting $J_0 = hC_0^s$ and $C_{out} = C_{steady}$ at the steady state, we have

$$J_{steady} = \frac{Q}{A} C_{out} \tag{19}$$

which is a model commonly used to calculate steady-state fluxes for dynamic chambers when C_{in} is assumed to be zero or negligible [*Denmead*, 1979; *Rolston*, 1986; *de Mello and Hines*, 1994; *Gao et al.*, 1997]. A more general form of (19) is

$$J_{steady} = \frac{Q}{A} (C_{out} - C_{in}) \tag{20}$$

In practice, C_{in} can be easily controlled, so it is either zero (or insignificant compared to C_{out}) or constant. Under such conditions it is not difficult to show that (20) can be also derived from the above analysis.

When the airstream stops (i.e., $Q = 0$), the dynamic chamber becomes a passive closed chamber discussed in the previous section. This can be shown by the fact that when $Q = 0$, equations (15), (16), (18), and (17) become (6), (7), (8), and (9), respectively, for the shallow closed chamber.

2.2.2. With effect of pressure deficit created by flowing air. When a pressure deficit is present within the chamber headspace, a volume air flux f_{sair} (L T^{-1}) will be induced from the covered soil matrix into the chamber. The target gas flux at the covered soil surface $J_g(t)$ has two components, i.e., a diffusive flux ($J_{diffusive}$, M L^{-2} T^{-1}) driven by the concentration gradient, and a convective flux ($J_{convective}$, M L^{-2} T^{-1}) along with f_{sair}, which can be written as

$$J_g(t) = J_{diffusive} + J_{convective} = h[C_0^s(t) - C^a(t)] + f_{sair}C_0^s(t) \tag{21}$$

where all the terms are defined previously. Similarly, a first-order nonhomogeneous differential equation for $C^a(t)$ can be obtained

$$\frac{dC^a(t)}{dt} + \frac{Q/A + h}{H} C^a(t) = \frac{h + f_{sair}}{H} C_0^s(t) \tag{22}$$

Using $C^a(0) = 0$, $C_0^s(t) = C_0^s$, and assuming a constant f_{sair}, we can obtain a solution for (22)

$$C^a(t) = \frac{hC_0^s}{Q/A + h}\left[1 - \exp\left(-\frac{Q/A + h}{H} t\right)\right] + \frac{f_{sair}C_0^s}{Q/A + h}\left[1 - \exp\left(-\frac{Q/A + h}{H} t\right)\right] \tag{23}$$

By introducing (23) into (21) the flux at the enclosed soil surface can be expressed as

$$J_g(t) = J_0\left\{1 - \frac{h}{Q/A + h}\left[1 - \exp\left(-\frac{Q/A + h}{H} t\right)\right]\right\} + f_{sair}C_0^s\left\{1 - \frac{f_{sair}C_0^s}{Q/A + h}\left[1 - \exp\left(-\frac{Q/A + h}{H} t\right)\right]\right\} \tag{24}$$

The first half on the right-hand side of (24), which is identical to (16), is the diffusion-driven flux. The second half of (24) represents the convective mass flow due to the effect of pressure deficit caused by the airstream in the chamber on the target gas flux. In the transient stage, both parts are functions of time (t) and the airflow rate (Q). When the chamber system reaches a steady state, or mathematically when $t \to \infty$, the concentration and flux become, respectively,

$$C^a(t \to \infty) = C_{steady} = \frac{h}{Q/A + h} C_0^s + \frac{J_{sair}}{Q/A + h} C_0^s \tag{25}$$

$$J_g(t \to \infty) = J_{steady} = J_0\left(1 - \frac{h}{Q/A + h}\right) + f_{sair}C_0^s\left(1 - \frac{h}{Q/A + h}\right) \tag{26}$$

The first part of (26) represents the flux of the target gas without the effect of the pressure deficit, while the second part of (26) reflects the effect of the pressure deficit. At steady state, both parts are functions of the airflow rate (Q). Again, if we combine (25) and (26) to solve for J_{steady}, assuming $f_{sair}A \ll Q$, we can obtain the steady-state flux model (19) or (20).

When the airflow is stopped (i.e., $Q = 0$), equations (23), (24), (25), and (26) will reduce to (6), (7), (8), and (9), respectively. Under this condition the dynamic chamber becomes a shallow closed chamber.

3. Simulation Results and Discussion

3.1. Behavior of Closed Chamber

To evaluate the general behavior of shallow closed chambers, we use (6) and (7) to show how the parameters (V/A and h) affect the concentration and flux as a function of time after chamber placement. A range of V/A from 10 to 40 cm is used in our simulation. This range covers the majority of the shallow closed chambers reported in the literature.

The transport coefficient (h) depends on the diffusivity of the target gas through the soil-atmosphere interface and the resistance nature of the interface. This coefficient can be expressed as

$$h \propto D^a \text{ or } h = \lambda D^a \tag{27}$$

where D^a (L^2 T^{-1}) is the diffusion coefficient of the target gas in the still air, and λ (L^{-1}) is a case-dependent constant reflecting the interfacial resistance. *Jury et al.* [1983] assumed a stagnant air layer at the soil surface and used a simple formula for estimating h

$$h = \frac{D^a}{d} \tag{28}$$

where d (L) is the thickness of the stagnant air layer. For simplicity and simulation purposes we assume that the thickness of the stagnant air layer above the enclosed soil surface will be equal to the height of the chamber, and the transport coefficient (h) is a function of the chamber height (H). It should be pointed out that the assumption of stagnant air in the closed chamber is valid only for shallow chambers without mixing. When mixing is provided inside the chamber, this assumption becomes invalid. However, our experiences have shown that as long as a closed chamber is shallow as defined previously, constant mixing should be avoided to eliminate unexpected adverse effects such as leaking and differentiation of flux at the enclosed soil surface. We select a range of D^a

from 0.05 to 0.25 $cm^2\ s^{-1}$. This range covers most of the volatile organic compounds and trace gases of environmental concern [*Schwarzenbach et al.*, 1993].

Plotting $C^a(t)/C_0^s$ and $J_g(t)/J_0$ as a function of time (t) using (6) and (7) shows the general behavior of shallow closed chambers with different V/A ratios or heights (H) when measuring flux of a typical VOC with a D^a of 0.10 $cm^2\ s^{-1}$, which is similar to benzene (D^a = 0.09 $cm^2\ s^{-1}$ at 20°C) (Figure 3). From Figure 3a it can be seen that the flux from the covered soil surface into the chamber headspace decreases with time. The smaller the V/A ratio or height (H) of the chamber, the more rapidly the flux decreases. When the chamber V/A ratio or the height increases, the flux approaches an approximate linear decrease, as shown by curves 3 and 4 in Figure 3a. Figure 3b shows that the target gas concentration in the chamber headspace increases with time but at different rates with different chamber V/A ratios or heights. When the chamber V/A ratio or the height increases, the target gas concentration in the chamber will show an approximate linear increase over time (curves 3 and 4 in Figure 3b). This linear increase is misleading because it seems to be resulted from a constant flux from the soil matrix into the chamber. However, this approximate linear increase in concentration is in fact associated with a decreasing flux, not a constant flux, as shown in Figure 3a.

The linear increase of the target gas concentration in the closed chambers has been experimentally observed in numerous investigations [e.g., *Matthias et al.*, 1980; *Nakayama*, 1990]. The observation has lead to the application of a linear model to calculate a "constant" or "average" flux. However, various chamber users, including those who observed the linear concentration increase in their experiments, have reported that the fluxes calculated by the linear model are underestimates of the actual fluxes [e.g., *Matthias et al.*, 1980; *Rolston*, 1986]. The simulation results discussed above can help explain a cause of this. Since the flux at the covered soil surface decreases with time after the chamber is placed, a "constant" or "average" flux calculated using the linear model is an underestimate of the actual flux present just before the chamber placement.

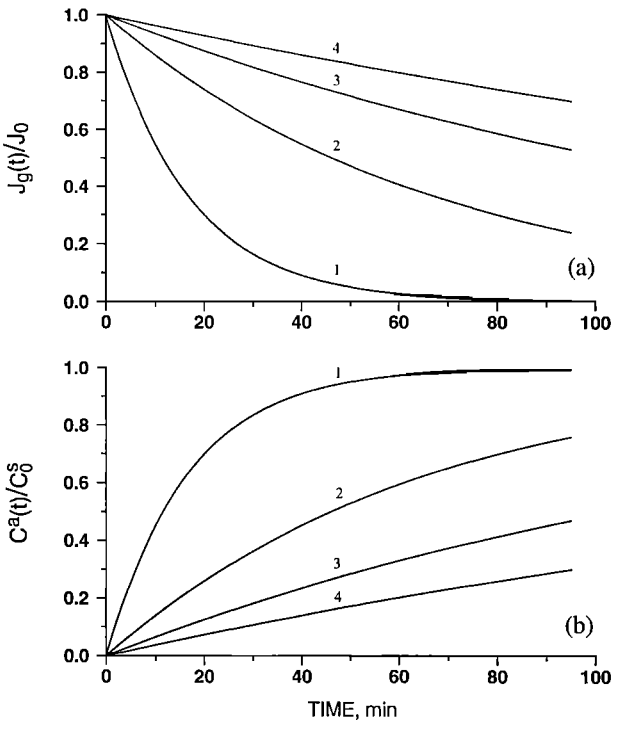

Figure 3. Behavior of shallow closed chamber with different V/A ratio (H). For curves 1, 2, 3, and 4 in the figure the V/A ratios are 10, 20, 30, and 40 cm, respectively.

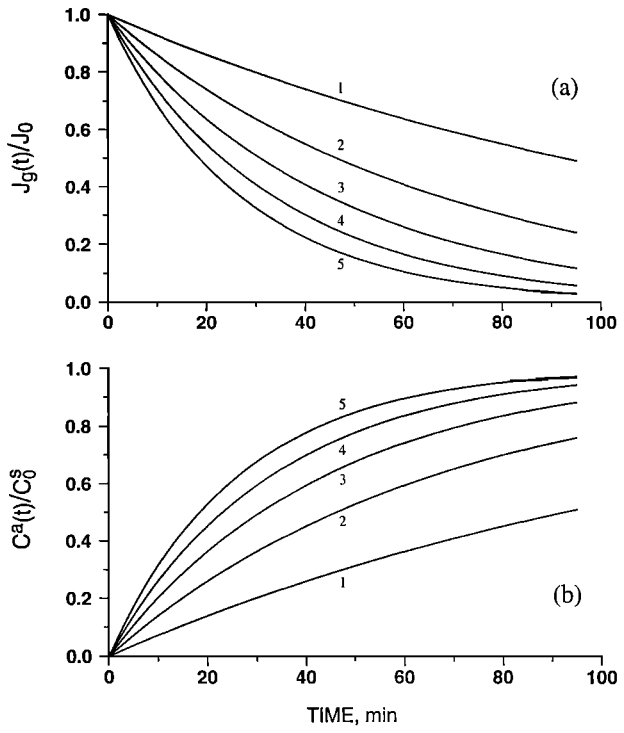

Figure 4. Behavior of a closed chamber with a V/A ratio of 20 cm when measuring gases with different D^a. For curves 1, 2, 3, 4, and 5 the D^a values are 0.05, 0.10, 0.15, 0.20, and 0.25 $cm^2\ s^{-1}$, respectively.

The behavior of a shallow closed chamber when measuring fluxes of different gases is shown in Figure 4. The chamber V/A ratio (or H) used is 20 cm. From Figure 4a it can be seen that the fluxes into the chamber also decrease with time. The fluxes of gases with higher diffusivities, such as soil trace gases like methane (D^a = 0.22 $cm^2\ s^{-1}$), decrease with time at faster rates than gases with lower diffusivities, such as VOCs (e.g., toluene, D^a = 0.08 $cm^2\ s^{-1}$). The comparison indicates that more mass of a trace gas will diffuse through the soil-air interface per unit time than that of a VOC under the same conditions. Thus a faster increase of the relative concentration (C^a/C_0^s) will occur in the chamber headspace when measuring a soil trace gas, as shown in Figure 4b. This will lead to a faster decrease of concentration gradient across the interface, which in turn leads to a faster decrease of the flux. Again, an approximate linear increase of the target gas concentration within the chamber headspace may be observed (e.g., curves 1 and 2 in Figure 4b). Such a linear increase, however, does not reflect a constant flux at the enclosed soil surface, as discussed above.

Equation (6) indicates that the relative concentration (C^a/C_0^s) will approach a value of 1 when the chamber placement time is extended long enough. This can be shown by the curves in Figures 3b and 4b if we extend the chamber placement time. On the other hand, the flux of the target gas at the enclosed soil surface will approach zero as the relative concentration approaches 1. A relative concentration of 1 implies that the concentration gradient across the soil-air interface be-

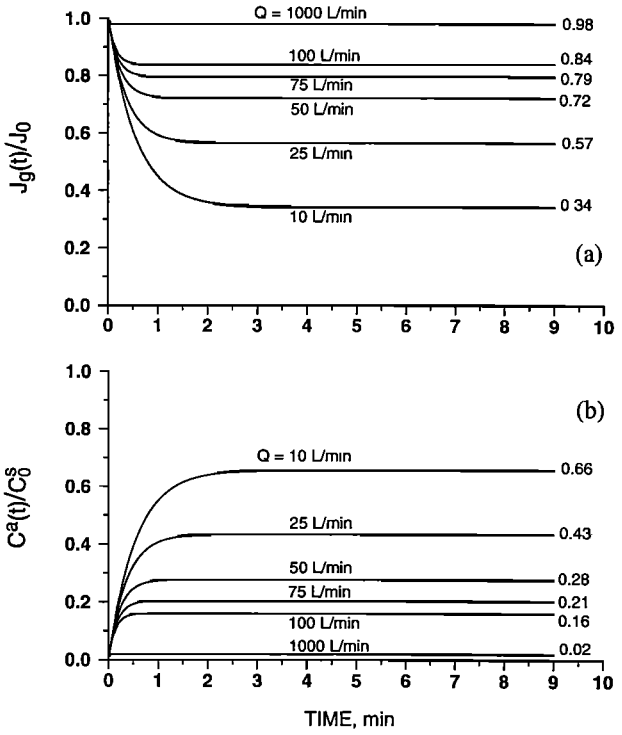

Figure 5. Effect of airflow rate (Q) on the transient stage behavior of a dynamic chamber with dimensions of W = 40 cm, L = 40 cm, and H = 10 cm.

comes zero, thus creating no (or zero) diffusive flux at the covered soil surface. Both Figures 3 and 4 suggest that the placement time of a closed chamber should be kept short, as long as the sensitivity of the analytical methods allows.

3.2. Behavior of Dynamic Chamber and Discussion

In the following simulation we first neglect the effect of pressure deficit created by the flowing air. We then include the effect of pressure deficit and compare how a dynamic chamber behaves under two scenarios.

3.2.1. Without effect of pressure deficit created by flowing air. We use (15) and (16) to simulate behavior of the dynamic chamber in the transient stage and (17) and (18) for the steady state. From (16) and (15) it can be seen that in the transient stage the flux of the target gas from the covered soil matrix decreases, while the concentration of the target gas in the chamber increases, with time after chamber placement. This indicates that the behavior of a dynamic chamber depends on the following physical factors: airflow rate (Q), interfacial transport coefficient (h) or diffusivity (D^a), and chamber dimension (A). Within a dynamic chamber we cannot assume that the stagnant air layer above the soil surface is equal to the chamber height since an airstream is continuously blowing over the enclosed soil surface. For simulation purpose we adopt a thickness of 0.5 cm for the stagnant air layer. This thickness has been used by various investigators to conduct successful simulation studies [*Jury et al.*, 1983; *Simunek and van Genuchten*, 1994]. In practice, the thickness of the stagnant air layer may change at different airflow rates. In a later paper, we will discuss in detail the effects of airstream in dynamic chamber on the stagnant air layer [*Gao and Yates*, 1998, this issue]. The effect of each physical factor on the chamber behavior is discussed below.

3.2.1.1. Airflow rate: Figure 5 is plotted using (15) and (16) and shows how the airflow rate affects the behavior of a dynamic chamber in the transient stage. Chamber dimensions used are 40 cm (length) by 40 cm (width) by 10 cm (height or thickness). A D^a value of 0.10 cm^2 s^{-1} is used to represent a typical VOC. For each case in Figure 5a the chamber system undergoes a short transient stage and reaches a steady state quickly after placement. At higher airflow rates (Q) the chamber system reaches the steady state more quickly. The short transition period implies that the commonly used chamber equilibration time of 15–30 min [e.g., *Denmead*, 1979; *Rolston*, 1986; *Valente et al.*, 1995] is reasonable. Figure 5 shows also that the relative flux $[J_g(t)/J_0]$ is always less than 1 even at a very high airflow rate (e.g., 1000 L min^{-1}). This indicates that when not considering the effect of pressure deficit, a dynamic chamber underestimates the initial flux prior to the chamber placement (i.e., J_0 at $t = 0$).

Figure 5b shows the relative concentration in the chamber headspace ($C^a(t)/C_0^s$) as a function of time. The concentration curves at various airflow rates show that the target gas concentration within a dynamic chamber will reach a constant value after a short transition period. When a dynamic chamber reaches the steady state, a constant concentration gradient is present at the enclosed soil surface under the given conditions. This concentration gradient is smaller than that outside the chamber, thus driving a diffusive flux smaller than the actual flux outside the chamber or just before the chamber placement.

3.2.1.2. Gas diffusivity: Simulation in Figure 6 shows the behavior of a dynamic chamber when measuring fluxes of gases

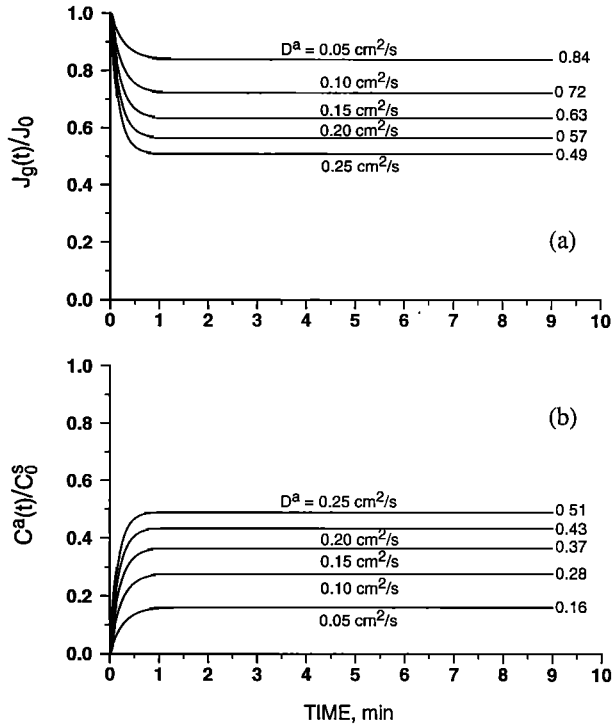

Figure 6. Effect of gas diffusivity (D^a) on the transient stage behavior of a dynamic chamber with dimensions of W = 40 cm, L = 40 cm, and H = 10 cm.

with different diffusivities. A chamber with a length of 40 cm, a width of 40 cm, and a height of 10 cm is used, and the airflow rate is set at 50 L min^{-1}. All five curves in Figures 6a and 6b show a relatively short transient stage. At steady sate under the same given conditions the relative flux of a gas with higher diffusivity is smaller than that of a gas with lower diffusivity. This is again due to the more rapid diffusive mass input into the chamber, leading to a higher steady-state concentration in the chamber headspace. As a result, the concentration gradient between the soil gas phase and the chamber headspace become smaller, thus driving a smaller diffusive flux.

3.2.1.3. Chamber dimension: The behavior of dynamic chamber as affected by chamber dimensions is plotted in Figure 7. The airflow rate is set at 50 L min^{-1}, and a D^a value of 0.10 cm^2 s^{-1} is used for a typical VOC. Figure 7 shows that at the same airflow rate, a smaller chamber will reach steady sate more rapidly than a larger chamber. After reaching the steady state at the same flow rate, the flux associated with a smaller chamber is closer to the initial flux (i.e., J_0).

3.2.1.4. Steady state: In practice, flux measurements by dynamic chambers are performed almost exclusively at the steady state. Figure 8 shows the steady-state behavior of a dynamic chamber when measuring two different gases, one with a D^a of 0.10 cm^2 s^{-1} (curves 1) and another with a D^a of 0.20 cm^2 s^{-1} (curve 2). From Figure 8 it can be seen that the steady-state flux underestimates the actual flux when the effect of pressure is not included, since the ratio of J_{steady}/J_0 is always less than 1. When the airflow rate (Q) is low, the degree of underestimate is severe. When Q increases, the underestimate becomes less severe. Second, the underestimate for a gas with a greater diffusivity (e.g., a trace gas) is more severe than that for a gas with a smaller diffusivity (e.g., a VOC) under the same conditions. The difference, however, becomes less noticeable as the airflow rate increases. Third, the steady-state flux approaches a relatively stable value that is close to the actual flux after the flow rate increases over a certain value. This indicates that increasing the airflow rate will produce a measured flux value that is closer to J_0.

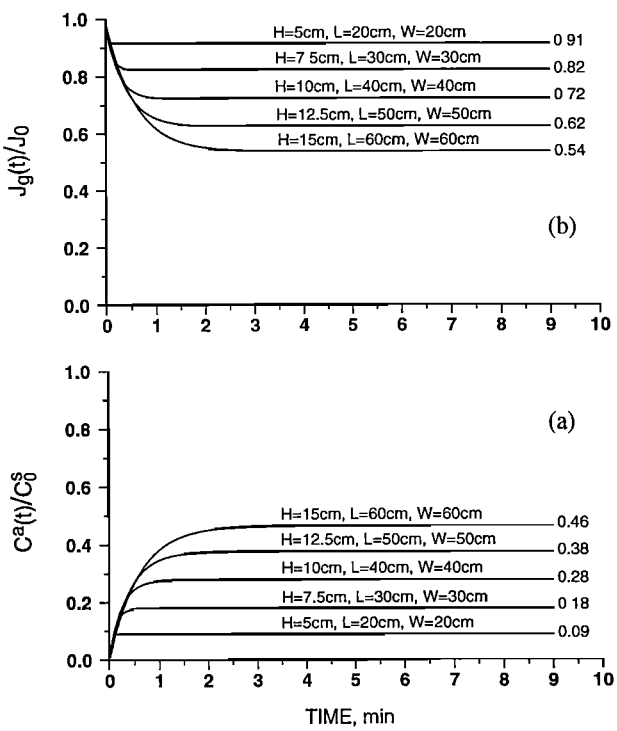

Figure 7. Effect of chamber dimension on the transient stage behavior of dynamic chamber when measuring a volatile gas with a D^a = 0.10 cm^2 s^{-1} at a airflow rate Q = 50 L min^{-1}.

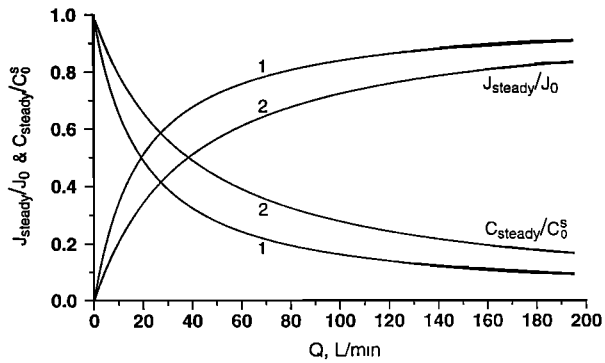

Figure 8. Steady-state behavior of a dynamic chamber when measuring two gases. Chamber dimensions: W = 40 cm, L = 40 cm, H = 10 cm. Curve 1: a VOC, D^a = 0.10 cm^2 s^{-1}. Curve 2: a trace gas, D^a = 0.20 cm^2 s^{-1}.

Figure 9 shows the steady-state behavior of two dynamic chambers when measuring a typical volatile organic gas (D^a = 0.10 cm^2 s^{-1}). Comparison of curve 1 and curve 2 in Figure 9 shows that a smaller chamber can obtain a steady-state flux closer to J_0 than a larger chamber at the same airflow rate. The difference becomes less noticeable as the airflow rate increases. The comparison implies that a smaller chamber may be more desirable than a larger one, unless the airflow rate for the larger chamber is increased accordingly.

3.2.2. With effect of pressure deficit. From (24) and (26) it can be seen that the effect of pressure deficit on the flux at the enclosed soil surface depends on f_{sair}, and the magnitude of the effect of pressure deficit can be represented by the term f_{sair}/h. For the simulation purpose we use Bernoulli's equation [*Vennard and Street*, 1975; *Giancoli*, 1984] to estimate the pressure difference between the airstream in the chamber and a stagnant zone at a depth of Z below the covered soil surface, which gives

$$\Delta P_Z = P_Z - P_0 = \tfrac{1}{2}\rho_a V_0^2 \tag{29}$$

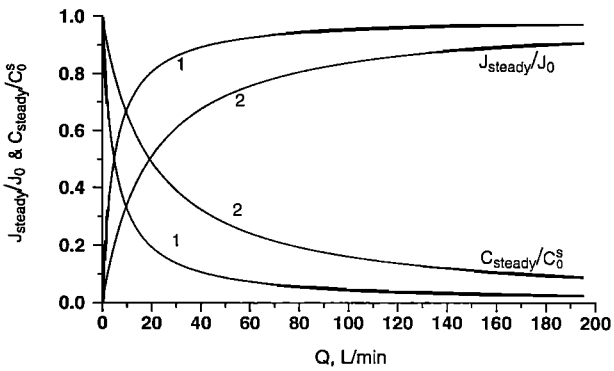

Figure 9. Steady-state behavior of two dynamic chambers when measuring a volatile gas with a D^a = 0.10 cm^2 s^{-1} at an airflow rate of Q = 50 L min^{-1}. Curve 1: a smaller chamber, W = 20 cm, L = 20 cm, H = 5 cm. Curve 2: a larger chamber, W = 40 cm, L = 40 cm, H = 10 cm.

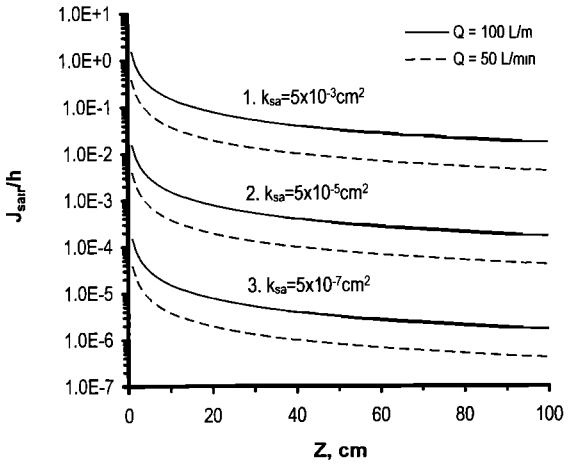

Figure 10. Effect of pressure deficit (f_{sair}/h) as a function of effective soil depth (Z). Chamber dimensions: W = 40 cm, L = 40 cm, H = 10 cm. Airflow rate: Q = 50 L min^{-1}.

where P_Z (Pa) and P_0 (Pa) are the pressures at the depth $z = Z$ (L) and the enclosed soil surface ($z = z_0 = 0$), respectively, ρ_a (M L^{-3}) is the density of the airstream, V_0 (L T-1) is the velocity of the airstream over the covered soil surface. For a dynamic chamber defined in Figure 2, V_0 can be estimated using Eq. (10), which gives

$$\Delta P_Z = \frac{\rho_a Q^2}{2W^2H^2} \tag{30}$$

where Q is the airflow rate and W and H are the chamber width and height, respectively.

If we assume ΔP_Z is linear from Z to the soil surface ($z = z_0 = 0$), the convective volume air flux f_{sair} can be formulated using an equation analogous to Darcy's equation [*Corey*, 1986]

$$f_{sair} = -\frac{k_{sa}}{\mu_{sa}}\frac{\Delta P_Z}{(z_0 - Z)} = \frac{k_{sa}\rho_a Q^2}{2\mu_{sa}W^2H^2Z} \tag{31}$$

where k_{sa} (L^2) is the permeability of the enclosed soil matrix, and μ_{sa} (ML^{-1} T^{-1}) is the viscosity of the soil air. Thus we have

$$\frac{f_{sair}}{h} = \frac{k_{sa}\rho_a Q^2}{2h\mu_{sa}W^2H^2Z} \tag{32}$$

To assess the effect of f_{sair}/h, we select a dynamic chamber with W = 40 cm, L = 40 cm, and H = 10 cm. We adopt a ρ_a of 1.3 mg cm^{-3} for the density of the airstream and a μ_{sa} of 0.18 mg cm^{-1} s^{-1} for soil air viscosity. We select three permeabilities to represent three different media: $k_{sa} = 3.0 \times 10^{-7}$ cm^2 for low permeability soils (e.g., silt and loam), $k_{sa} = 3.0 \times 10^{-5}$ cm^2 for moderate permeability soils (e.g., sands), and $k_{sa} = 3.0 \times 10^{-3}$ cm^2 for highly permeable media such as gravels and mulches. The property values selected here are obtained or estimated from the data reported by *Kimball and Lemon* [1971], *Clapp and Hornberger* [1978], and *Massmann* [1989]. Again, we use (28) to estimate the interfacial transport coefficient (h). We use a D^a value of 0.10 cm^2 s^{-1} for a typical VOC and a d of 0.5 cm to obtain an h value of 0.2 cm s^{-1}.

Figure 10 is plotted using (32) to show f_{sair}/h as a function of soil depth (Z) for the three media specified above. A constant airflow rate of 100 L min^{-1} is employed. This value is in the higher range of airflow rates reported in the literature. Figure 10 shows that the f_{sair}/h ratio is very small for the less permeable media under the given conditions. For the permeable medium ($k_{sa} = 3.0 \times 10^{-3}$ cm^2), f_{sair}/h is significant when Z is small. However, f_{sair}/h becomes less significant as the soil depth increases. For example, f_{sair}/h is less than 0.1 (or 10%) when the soil depth is 10 cm or greater. In practice, this condition (i.e., $Z \geq 10$ cm) can be approximated by applying a chamber collar inserted to a depth of 10 cm or deeper, as indicated in Figure 2b.

Figure 11 shows the ratio of f_{sair}/h as a function of chamber airflow rate (Q). A reference (or effective) soil depth of 10 cm and the same chamber dimensions are used. It can be seen that the ratio of f_{sair}/h is insignificant for the less permeable media even at a very high airflow rate (e.g., 500 L min^{-1}). The f_{sair}/h ratio is significant for the permeable medium when the chamber is operating at high airflow rates. For example, the values of this ratio are approximately 0.5 and 3.5 when the airflow rates are 200 and 500 L min^{-1}, respectively. However, the f_{sair}/h ratio becomes again insignificant when the airflow rate decreases to below 100 L min^{-1} (curve 1 in Figure 11).

We can further estimate the effect of the pressure deficit caused by flowing air on the steady-state behavior of dynamic chambers. Figure 12 is plotted using (25) and (26) to simulate the steady-state behavior of a dynamic chamber when measuring fluxes of a typical VOC at soil surface. The curves in Figure 12 show J_{steady}/J_0 and C_{steady}/C_0^s as functions of chamber airflow rate (Q) when the chamber is operating on the three media specified previously. The chamber dimensions stay the same (i.e., W = 40 cm, L = 40 cm, H = 10 cm), and an effective soil depth (Z) of 10 cm is used. Other property values are the same as described after (32). The curves of the relative flux in Figure 12 show clearly that whether the dynamic chamber overestimates or underestimates the actual flux depends on the chamber airflow rate (Q) and the soil type as well. For low permeability soils, such as silty, loamy, and clayey soils, the dynamic chamber is likely to underestimate the actual flux even at very high airflow rates (Figure 12a). For media with high air permeability, such as very coarse sands, gravels, and coarse-textured mulches encountered in agricultural and forest soils, a much lower airflow rate may lead to overestimate of the flux, as shown in Figure 12c.

3.2.3. Relative significance of effect of pressure deficit. Since a dynamic chamber can reach a steady state in a relatively short period of time (Figures 5, 6, and 7) and flux mea-

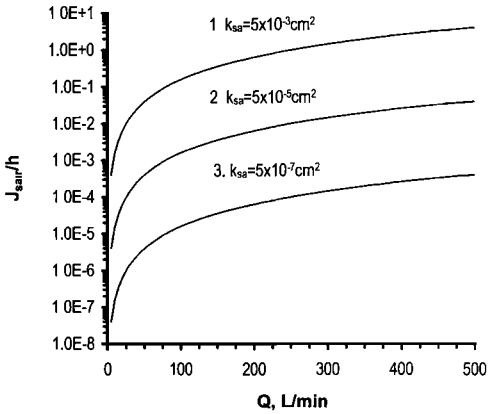

Figure 11. Effect of pressure deficit (f_{sair}/h) as function of chamber airflow rate (Q). Effective soil depth: Z = 10 cm. Chamber dimensions: W = 40 cm, L = 40 cm, H = 10 cm.

surements are almost always made at the steady state, we are most interested in the behavior of dynamic chamber at steady state. If we compare the results of our simulations with and without taking into account the effect of pressure deficit caused by the flowing air, some meaningful points can be drawn for practical chamber operation.

First, when operating on soils with relatively low permeability such as clayey, loamy, and silty soils, a dynamic chamber is likely to underestimate the actual flux as long as the chamber airflow rate is maintained relatively low (Figures 8, 9, and 12). In field applications, airflow rates of several hundred liters per minute may not be practically feasible or desirable. Flow rates of less than 100 L min^{-1} are most often reported in the literature. Under such conditions, whether or not to include the effect of pressure deficit created by flowing air may not make significant difference.

Second, when a dynamic chamber is used on highly permeable media (such as coarse sands, gravels, and coarse-textured mulches), consideration of the effect of pressure deficit may become important, as shown in Figure 12c. For example, when a dynamic chamber is operating on a highly permeable soil with an airflow rate of 200 L min^{-1}, a measured VOC flux would be considered to underestimate the true flux by approximately 10% if the effect of pressure deficit were not included (curve 1 in Figure 8). This flux, however, may be actually an overestimate by about 10% due to the effect of pressure deficit caused by the flowing air (Figure 12c). It should be noted that for high permeability soils the effect of pressure deficit can be ignored as well when the chamber is operating at a very low airflow rate.

Third, at very low airflow rates, a dynamic chamber may always underestimate the real flux, regardless of the type of medium. All steady-state curves in Figure 12 show that the underestimate of the real flux at steady state may be severe at very low airflow rates (Q). The gas flux from the covered soil matrix into the chamber is likely to be governed mainly by diffusion, and the mass flow induced by the pressure deficit may become insignificant and negligible. It can be seen also that under such conditions the chamber behavior is very sensitive to the airflow rate (Q) in terms of the flux measured at steady state. A flow rate difference of several liters per minute may lead to a difference of several percent or even greater in the flux being measured. This suggests that operations of a dynamic chamber at very low airflow rates is to be avoided in field applications.

3.2.4. Pressure difference caused by other factors. It should be pointed out that the cause of the pressure deficit discussed so far in this paper is limited solely to the flowing air through the chamber, so the Bernoulli's equation can be used to estimate this pressure deficit. In practice, the airstream through a dynamic chamber is driven either by a vacuum at the outlet side or by an air blower at the inlet side, although the latter is used much less often. *Kanemasu et al.* [1974] reported that sucking air at the outlet and blowing air at the inlet created opposite pressure differences within their chamber, although the airflow rate was the same under the two scenarios. In our recent laboratory study, we have observed that a vacuum from the outlet side of the chamber can create a pressure deficit greater than that estimated by Bernoulli's equation [*Gao and Yates*, this issue]. We will discuss this vacuum-induced pressure deficit in detail in a later paper.

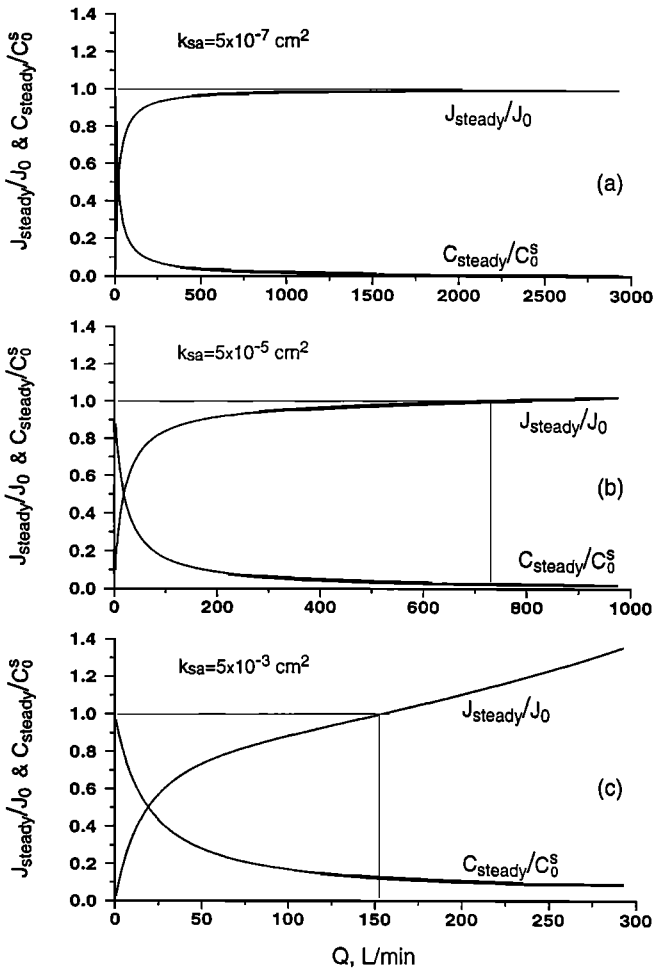

Figure 12. Steady-state behavior of a dynamic chamber on three media when the effect of pressure deficit caused by flowing air is included. Effective soil depth: Z = 10 cm. Chamber dimensions: W = 40 cm, L = 40 cm, and H = 10 cm.

4. Concluding Remarks

Our simulation of the behavior of shallow passive (or closed) flux chambers suggests that the chamber V/A ratio or height H should be large enough to minimize the problem of relatively rapid decrease of the flux at the enclosed soil surface. With a large V/A ratio or H, a well-mixed condition in the chamber may not be guaranteed. Thus installation of a mixing device (such as a small low-speed fan) may become necessary. When using a shallow closed chamber with a relatively large V/A ratio or H, the concentration data obtained in the chamber headspace may show a linear increase with time during a relatively short placement period. This linear behavior, however, is an artifact of the timescale of the observation. It may mislead one to assume that a simple linear model may be adequate for determining the flux. Since the flux calculated by the linear model will underestimate the actual flux, nonlinear flux models [e.g., *de Mello and Hines*, 1994] should be considered. The chamber placement time may need to extend to obtain nonlinear concentration data for using those nonlinear models.

Dynamic chambers have been generally considered to result in overestimates of the actual flux. However, simulations in this study show that these chambers may lead to overestimates, as well as underestimates of the actual flux.

When operating on low permeability soils, such as loamy and clayey soils, a dynamic chamber is likely to underestimate the actual flux when using (19) or (20) to calculate the steady-state flux, except when the chamber airflow rate is very high. However, an extremely high flow rate may not be feasible in practical applications. When operating on highly permeable soils, such as coarse sands, gravels, and mulches, a dynamic chamber may overestimate the real flux, depending on the actual airflow rate through the chamber and the air permeability of the soil matrix involved.

When the effect of pressure deficit caused by the flowing air is considered, the analysis and simulation results for the dynamic chambers presented in this study are valid only for the chamber defined in Figure 2. The special design of this chamber allows a simple airflow pattern within the chamber [*Gao et al.*, 1997]. This simple pattern makes it possible to evaluate the chamber behavior as a function of airflow rate (Q), or Q/A ratio, and the flowing air velocity (V_0). When the effect of pressure deficit caused by the airstream is not considered to be a significant factor, the simulation results in this study may be used as reference information for dynamic chambers with other design structures.

Acknowledgments. The authors thank M. V. Yastes, W. A. Jury, and W. F. Spencer for their valuable suggestions and comments provided while this study was conducted.

References

Balfour, W. D., C. E. Schmidt, and B. M. Eklund, Sampling approaches for the measurement of volatile compounds a hazardous waste sites, *J. Hazard. Mat.*, *14*, 135–148, 1987.

Cicerone, R. J., and J. D. Shetter, Sources of atmospheric methane: Measurements in rice paddies and a discussion, *J. Geophys. Res.*, *86*, 7203–7209, 1981.

Clapp, R. B., and G. M. Hornberger, Empirical equations for some soil hydraulic properties, *Water Resour. Res.*, *14*, 601–604, 1978.

Clendening, L. D., A field mass balance study of pesticide volatilization, leaching and persistence, Ph.D. dissertation, Dep. of Soil and Environ. Sci., Univ. of Calif., Riverside, CA, 1988.

Corey, A. T., Air permeability, in *Methods of Soil Analysis, 1, Physical and Mineralogical Methods*, 2nd ed., edited by A. Klute, pp. 1121–1136, Agron. Monogr. 9. ASA and SSSA, Madison, Wisc., 1986.

de Mello, W. Z., and M. E. Hines, Application of static and dynamic enclosures for determining dimethyl sulfide and carbonyl sulfide exchange in Sphagnum peatlands: Implication for magnitude and direction of flux, *J. Geophys. Res.*, *99*, 14,601–14,607, 1994.

Denmead, O. T., Chamber system for measuring nitrous oxide emission from soils in the field, *Soil Sci. Soc. Am. J.*, *43*, 89–95, 1979.

Denmead, O. T., and M. R. Raupach, Methods for measuring atmospheric gas transport in agricultural and forest systems, in *Agricultural Ecosystem Effects on Trace Gases and Global Climate Change*, pp. 19–43, ASA Spec. Publ. 55. ASA, CSSA, and SSSA, Madison, WI, 1993.

Dupont, R. R., and J. A. Reinman, Evaluation of volatilization of hazardous constituents at hazardous waste land treatment sites, *Proj. Rep. EPA/600/S2-86/071*, U.S. Environ. Prot. Agency, R. S. Kerr Environ. Res. Lab., Ada, OK, 1986.

Frankenberger, W. T., Jr., and U. Karlson, Microbial volatilization of selenium from soils and sediments, in *Selenium in the Environment*, edited by W. T. Frankenberger Jr. and S. Benson, pp. 369–387, Marcel Dekker, Inc., New York, 1994.

Fukui, Y., and P. V. Doskey, An enclosure technique for measuring non-methane organic compound emissions from grassland, *J. Environ. Qual.*, *25*, 601–610, 1996.

Gao, F., and S. R. Yates, Laboratory study of closed and dynamic flux chambers: Experimental results and implications for field application, *J. Geophys. Res.*, this issue.

Gao, F., S. R. Yates, M. V. Yates, G. Gan, and F. F. Ernst, Design, fabrication and application of a dynamic chamber for measuring gas emissions from soil, *Environ. Sci. Technol.*, *31*, 148–153, 1997.

Giancoli, D. C., *General Physics*, Prentice-Hall, Inc., Englewood Cliffs, N. J., 1984.

Healy, R. W., R. G. Striegl, T. F. Russell, G. L. Hutchinson, and G. P. Livingston, Numerical evaluation of static-chamber measurements of soil-atmosphere gas exchange: Identification of physical processes, *Soil Sci. Soc. Am. J.*, *60*, 740–747, 1996.

Holzapfel-Pschorn, A., and W. Seiler, Methane emission during a vegetation period from an Italian rice paddy, *J. Geophys. Res.*, *91*, 11,803–11,814, 1986.

Hutchinson, G. L., and A. R. Mosier, Improved soil cover method for field measurement of nitrous oxide fluxes, *Soil Sci. Soc. Am. J.*, *45*, 311–316, 1981.

Jury, W. A., J. Letey, and T. Collins, Analysis of chamber methods used for measuring nitrous oxide production in the field, *Soil Sci. Soc. Am. J.*, *46*, 250–256, 1982.

Jury, W. A., W. F. Spencer, and W. J. Farmer, Behavior assessment model for trace organics in soil, I, Model description, *J. Environ. Qual.*, *12*, 558–563, 1983.

Kanemasu, E. T., W. L. Powers, and J. W. Sij, Field chamber measurements of CO_2 flux from soil surface, *Soil Sci.*, *118*, 233–237, 1974.

Kimball, B. A, and E. R. Lemon, Air turbulence effects upon soil gas exchange, *Soil Sci. Soc. Am. Proc.*, *35*, 16–21, 1971.

Massmann, J. W., Applying groundwater flow models in vapor extraction system design, *J. Environ. Eng., ASCE*, *115*, 129–149, 1989.

Matthias, A. D., A. M. Blackmer, and J. M. Bremner, A simple chamber technique for field measurement of emissions of nitrous oxide from soil, *J. Environ. Qual.*, *9*, 252–256, 1980.

Moore, T. R., and N. T. Roulet, A comparison of dynamic and static chambers for methane emission measurements from subarctic fens, *Atmos. Ocean*, *29*, 102–109, 1991.

Mosier, A. R., Chamber and isotope techniques, in *Exchange of Trace Gases Between Terrestrial Ecosystems and the Atmosphere*, edited by M. O. Andreae and D. S. Schimel, pp. 175–187, John Wiley, New York, 1989.

Nakayama, F. S., Soil respiration, *Remote Sens. Rev.*, *5*, 311–321, 1990.

Rochette, P., E. G. Gregorich, and R. L. Desjardins, Comparison of static and dynamic closed chambers for measurement of soil respiration under field conditions, *Can. J. Soil Sci.*, *72*, 605–609, 1992.

Rolston, D. E., Gas flux, in *Methods of Soil Analysis*, 1, *Physical and Mineralogical Methods*, 2nd ed., edited by A. Klute, pp. 1103–1119, *Agron. Monogr. Ser.*, vol. 9, Am. Natl. Stand. Inst., New York, 1986.

Sanders, P. F., M. M. McChesney, and J. N. Seiber, Measuring pesticide volatilization from small surface areas in the field, *Bull. Environ. Contam. Toxicol.*, *35*, 569–575, 1985.

Schwarzenbach, R. P., P. M. Gschwend, and D. M. Imboden, *Environmental Organic Chemistry*, John Wiley, New York, 1993.

Valente, R. J., F. C. Thornton, and E. J. Williams, Field comparison of static and flow-through chamber techniques for measurement of soil NO emission, *J. Geophys. Res.*, *100*, 21,138–21,147, 1995.

Vennard, J. K., and R. L. Street, *Elementary Fluid Mechanics*, 5th ed, John Weily, New York, 1975.

Wesely, M. L., D. H. Lenschow, and O. T. Denmead, Flux measurement techniques, in *Global Tropospheric Chemistry: Chemical Fluxes in the Global Atmosphere*, edited by D. H. Lenschow and B. B. Hicks, pp. 31–46, Natl. Cent. for Atmos. Res., Boulder, Colo., 1989.

Woodrow, J. E., and J. N. Seiber, Two chamber methods for the determination of pesticide flux from contaminated soil and water, *Chemosphere*, *23*, 291–304, 1991.

Yagi, K., J. Williams, N.-Y. Wang, and R. J. Cicerone, Agricultural soil fumigation as a source of atmospheric methyl bromide, *Proc. Natl. Acad. Sci.*, *90*, 8420–8423, 1993.

Yates, S. R., J. Gan, F. F. Ernst, and D. Wang, Methyl bromide emissions from a covered field, III, Correcting chamber flux for temperature, *J. Environ. Qual.*, *25*, 892–898, 1996.

F. Gao (corresponding author), Air Quality Management Section, Delaware Dept. of Natural Resources and Environmental Control, Dover, DE 19901. (e-mail: "fgao@dnrec.state.de.us").

S. R. Yates, Physics and Pesticide Unit, U.S. Salinity Lab., U.S. Department of Agriculture, 450 W. Big Springs Rd., Riverside, CA 92507.

(Received May 27, 1997; revised March 20, 1998;
accepted April 15, 1998.)